

Fast Linear Least-Squares Method for Ultrasound Attenuation and Backscatter Estimation

Jasleen Birdi^{a,b,*}, Arun Muraleedharan^{a,b,1}, Jan D'hooge^a and Alexander Bertrand^b

^aDepartment of Cardiovascular Sciences, KU Leuven, Leuven, Belgium

^bDepartment of Electrical Engineering (ESAT), KU Leuven, Leuven, Belgium

ARTICLE INFO

Keywords:

Quantitative Ultrasound
Attenuation Estimation
Backscatter Estimation
Least Squares
Gain Calibration

ABSTRACT

The ultrasonic attenuation and backscatter coefficients of tissues are relevant acoustic parameters due to their wide range of clinical applications. In this paper, a linear least-squares method for the estimation of these coefficients in a homogeneous region of interest based on pulse-echo measurements is proposed. The method efficiently fits an ultrasound backscattered signal model to the measurements in both the frequency and depth dimension simultaneously at a low computational cost. It is demonstrated that the inclusion of depth information has a positive effect particularly on the accuracy of the estimated attenuation. The sensitivity of the attenuation and backscatter coefficients' estimates to several predefined parameters such as the window length, window overlap and usable bandwidth of the spectrum is also studied. Comparison of the proposed method with a benchmark approach based on dynamic programming highlights better performance of our method in estimating these coefficients, both in terms of accuracy and computation time. Further analysis of the computation time as a function of the predefined parameters indicates our method's potential to be used in real-time clinical settings.

1. Introduction

Quantitative ultrasound (QUS) methods are primarily used to measure variables by which one can quantitatively assess the acoustic properties of tissues [1, 2]. Among these variables, attenuation and backscatter coefficients draw much attention specifically because of their wide variety of clinical applications, whether it be monitoring kidney functioning in the body [3] or guiding prostate biopsies [4]. In particular, attenuation estimation has been used to differentiate fatty liver from normal liver as well as to diagnose chronic liver diseases [5, 6, 7]. The attenuation measurements have also shown diagnostic value in areas including the trabecular and cortical bone [8, 9], placentas [10], to name a few. An accurate estimate of the attenuation coefficient also allows to perform more accurate time gain compensation (TGC) in ultrasound images [11]. Similarly, backscatter estimation has proved to be beneficial in classifying masses as benign or malignant in organs including the eyes [12] and breast [13].

Due to these promising applications of the acoustic attenuation and backscatter coefficient in ultrasonic tissue characterization, it is important to estimate these parameters accurately. Furthermore, when the estimated attenuation coefficient is used for TGC, it has to be estimated in real time [14]. It is then pertinent to develop estimation methods, especially for the attenuation coefficient, which are computationally fast.

The problem of quantitative tissue parameters estimation has already been addressed for a few decades and several methods have been proposed. Classical spectral shift methods [15, 16, 17, 18] estimate the attenuation coefficient using the measurement of the center frequency downshift of a

Gaussian spectrum. Spectral difference methods [19, 20, 21] present another fundamental approach to estimate the attenuation coefficient by measuring the log-intensity decay in the backscattered signals at each frequency. Within this context, reference phantom methods (RPM) [22] are commonly used for attenuation and backscatter estimation because of their capability to correct for system-dependent diffraction effects. More recently, hybrid techniques have also been proposed that combine spectral shift and spectral difference methods to get more accurate attenuation coefficient estimates [23, 24].

Another class of approaches for tissue parameters estimation is based on minimizing the squared error between the measured spectrum of the backscattered signal and a parametric model of the spectrum. One such method for attenuation estimation was proposed in [25], solving a non-linear least squares problem to obtain *local* attenuation estimates. An exhaustive search was performed over a range of possible attenuation coefficients, making it computationally time consuming and hence, unsuitable for real-time applications. Simultaneous estimation of the attenuation and backscatter coefficients was performed in [26] by means of a reference phantom of which these coefficients were known. The authors minimized the squared error between the log-spectra of the model and the measurements, while constraining the estimates to be in a physical range. This method was shown to obtain more accurate estimates than obtained by the standard RPM. Nonetheless, the method focused on computing only an effective attenuation coefficient for the tissue path till the depth of interest. As such, the methods in both [25] and [26], did not exploit the depth information directly. Working in this direction, some regularized approaches have been developed recently that aim to enforce piece-wise continuity of the underlying tissue properties using a suitable regularization term in the cost function to be minimized. For instance, the authors in [27] regularized the attenuation map using

*Corresponding author at: Lab on Cardiovascular Imaging and Dynamics, Department of Cardiovascular Sciences, KU Leuven, Leuven, Belgium.

✉ jasleen.birdi@kuleuven.be (Jasleen Birdi)

¹Joint first authors

the isotropic total variation term, obtaining estimates with high accuracy and precision. However, this method was proposed only for attenuation estimation. Estimation of both the backscatter and attenuation coefficients with ℓ_2 norm depth-regularization in [28] and later on with ℓ_1 norm regularization in [29] was performed using dynamic programming (DP) to solve the considered regularized least squares based cost function. While this DP based approach was demonstrated to perform better than the least squares method in [26], it might not be feasible for real-time applications due to the computational lag experienced while evaluating the cost function at each depth for all the possible values of the parameters within the user-specified search range.

In this paper, we propose a fast and low-cost linear least-squares method for attenuation and backscatter estimation in a homogeneous region of interest (ROI). One of the key points of the proposed approach lies in fitting the linearized backscattered signal model in both the frequency and depth dimension simultaneously, thereby exploiting more information from the physical model. More importantly, writing the linearized model as a matrix equation allows to compute the coefficients of interest non-iteratively from a single-shot closed-form expression, making our method useful for real-time applications.

The rest of the paper is organized as follows. In section 2, starting with the backscatter signal model, we provide a brief overview of the approaches relevant to the current study, which is followed by the description of the proposed method. In section 3, we detail the simulated and experimental phantom-based data recordings as well as the analysis and the validation methodology. The results of this analysis are reported in section 4. The influence of window length, window overlap and usable bandwidth on the parameters estimation is also analyzed. Computation time sensitivity of the proposed approach to these parameters is also studied. A discussion is provided in section 5, and the paper is concluded in section 6.

Note: A conference precursor of this work was published in [30] for the case of attenuation estimation, validated only on simulated data. The current paper also includes backscatter estimation, and adds a more extensive analysis on parameter sensitivity, as well as an in-vitro validation. Furthermore, it is noted that during the write-up of this article, another independent work adopting a highly similar approach, referred to as ALGEBRA, has been published [31]. Our method and ALGEBRA were independently developed, yet share the same core principles and only deviate from each other through a few subtle differences. Therefore, the current paper can be viewed as an independent validation and confirmation of the results in [31] and vice versa. Moreover, we add to [31] by also providing a sensitivity analysis on some of the hyperparameters, such as the analysis window length, window overlap, and bandwidth of the spectral fit. Finally, we also demonstrate how the method can be used either with or without a reference phantom, and validate both cases.

2. Least Squares Attenuation & Backscatter Estimation

2.1. Signal Model

Consider the propagation of an acoustic wave within an isotropic and a homogeneous medium, generated by means of an acoustic transducer. Using the Born approximation of weak scattering, the magnitude spectrum of the backscattered signal, $|S(f, z)|$, where f and z denote frequency and depth, respectively, can be expressed as [26]

$$|S(f, z)| = |P(f)| D(f, z) A(f, z) B(f), \quad (1)$$

where $|P(f)|$ represents a combined effect of the electrical excitation and the transducer effects, $D(f, z)$ denotes the diffraction effects, $A(f, z)$ represents the cumulative attenuation of the sample, and $B(f)$ represents the backscatter coefficient (BSC).

In order to obtain the spectrum $P(f)$, a pulse-echo reflector measurement can be performed and the resulting (measured) spectrum is denoted by $\tilde{P}(f)$. The shape of the spectrum $\tilde{P}(f)$ is assumed to be known up to an unknown positive scaling factor G' , referred to here as the *gain calibration factor*, which accounts for the uncertainty in how much energy is actually transmitted into the medium. This implies $P(f) = G' \tilde{P}(f)$ in equation (1). Further, the attenuation of the sample, $A(f, z)$ can be expressed as an exponentially decaying function. For most soft tissues, we can assume a linear frequency dependence of the attenuation [37], resulting in $A(f, z) = \exp(-2\alpha f z)$, where α is the attenuation coefficient to be estimated. Finally, the backscatter coefficient is given by $B(f) = B_0 f^\mu$, where B_0 is a constant for a homogeneous medium and f^μ is the frequency-dependent backscatter term with μ taking a non-negative value [38]. The constant term B_0 can be integrated into the gain calibration factor resulting in the following measurement model¹:

$$|S(f, z)| = G |\tilde{P}(f)| D(f, z) \exp(-2\alpha f z) f^\mu, \quad (2)$$

where $G = G' B_0$.

2.2. Related prior art

It can be observed from equation (2) that the attenuation term has a depth-dependence. Existing methods like [25] deal with the local attenuation estimation at each depth within the probed region. To be more precise, the attenuation estimation for a homogeneous medium was performed in [25] using a non-linear least squares (NLS) framework where an optimum attenuation coefficient was computed at each depth by minimizing the squared error between the model (ignoring the diffraction effects and the backscatter coefficient in (2)) and the spectrum of the recorded backscattered signal at that particular depth. For the estimation, a sliding window technique was used, dividing the z axis into M overlapping windows

¹While we work with the magnitude spectrum of the backscattered signal, it is straightforward to relate the parameters of interest in this model with those in the backscattered power spectrum model (represented here by $(\cdot)'$) [26]. In the latter case, we will have $A'(f, z) = \exp(-4\alpha f z)$, $\mu' = 2\mu$ and $B'_0 = B_0^2$.

as shown in the top plot of fig.1. For every j th window, with $j = 1 \dots M$, z_j was chosen as the mid-point and the estimate, $\hat{\alpha}_j$ of α_j at depth z_j was obtained by an exhaustive search within a range of 0 to 2 dB/cm/MHz. Note that this introduces a trade-off between the accuracy and computation time, where a coarser gridding of the range results in faster searches yet with larger discretization errors on α . The final estimate of α was obtained by averaging the local estimates $\hat{\alpha}_j$ over all M windows, i.e.

$$\bar{\alpha} = \frac{\sum_{j=1}^L \hat{\alpha}_j}{M}. \quad (3)$$

Since all $\hat{\alpha}_j$'s were estimated locally (for each z_j separately), the depth dependency of the model (2) is not exploited to 'couple' the different $\hat{\alpha}_j$'s.

The approach in [26] dealt with the problem in the log-transformed domain to obtain a linear model. Here, we describe this method briefly, which was based on RPM, as our method re-uses some of its ingredients. Basically, it involves taking the ratio of the power spectrum of the backscattered signals from the sample of interest to that from the same depth of a reference phantom of which the attenuation coefficient α_r and the backscatter coefficient - its constant term $(B_0)_r$ and the exponent μ_r of the frequency-dependent term are known. Using the same transducer and imaging settings for the reference phantom and the actual sample under test, the ratio in terms of the magnitude spectrum can be deduced from equation (2) as

$$\frac{|S_s(f, z)|}{|S_r(f, z)|} = \frac{(B_0)_s}{(B_0)_r} \exp \{-2(\alpha_s - \alpha_r) f z\} f^{\mu_s - \mu_r}, \quad (4)$$

where the subscripts s and r refer to the sample and reference phantom, respectively. The diffraction effects $D(f, z)$ get cancelled out in this ratio under the assumption that both media have the same diffraction characteristics, whereas the term $\tilde{P}(f)$ vanishes due to the same transducer settings in the two cases. Furthermore, this also implicitly assumes that the gain G' is the same for the target medium and the reference phantom.

Equation (4) can be linearized in terms of the parameters of interest by applying a logarithmic transform on both sides of the equation. Doing so, we obtain:

$$\bar{Q}(f, z) = \log \frac{|S_s(f, z)|}{|S_r(f, z)|} = \log \bar{B}_0 - 2\bar{\alpha} f z + \bar{\mu} \log f, \quad (5)$$

where \log denotes the natural logarithm and

$$\bar{B}_0 = (B_0)_s / (B_0)_r, \quad (6)$$

$$\bar{\alpha} = \alpha_s - \alpha_r, \quad (7)$$

$$\bar{\mu} = \mu_s - \mu_r. \quad (8)$$

The linear equation (5) is typically used to estimate the unknown coefficients of interest. Once these values are obtained, it is straightforward to retrieve the corresponding coefficients for the sample using equations (6)-(8) as the values for the reference phantom are already known.

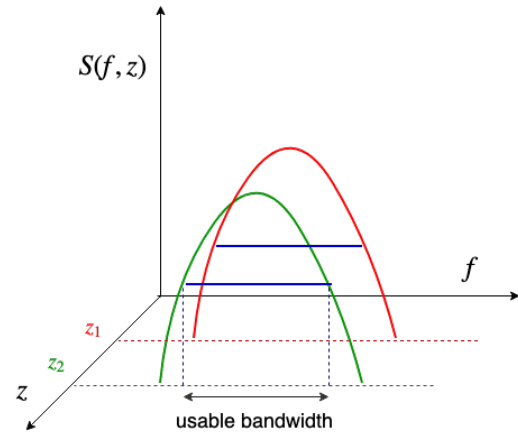
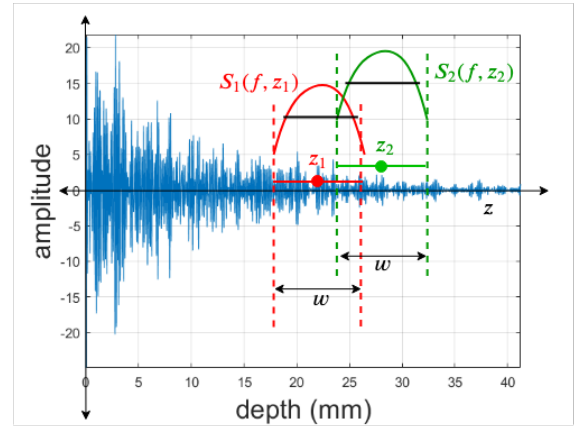


Figure 1: Top: Sliding window analysis for obtaining the magnitude spectrum from time windows at two consecutive locations z_1 (red) and z_2 (green), from the backscattered signal in time domain. Bottom: The blue lines below the peak of each spectrum represent the usable frequency range that is taken into consideration for parameter estimation.

In order to simultaneously estimate the attenuation and backscatter coefficients from (5), the authors in [26] considered a constrained linear least squares approach, which could be solved iteratively using off-the-shelf least squares solvers. Concerning the attenuation coefficient, an effective estimate was obtained at each considered depth by fitting the model over the entire frequency band of the backscattered signal spectrum, and the dependencies in the model across the z -axis were not exploited.

2.3. Aim of the paper

Our aim here is to fully exploit the depth information in the backscattered signal model and propose a fast, global attenuation and backscatter coefficient estimation methodology. The proposed strategy assumes the target coefficients to be constant in a ROI. It solves a linear least squares problem in which a single attenuation and backscatter coefficient are fit over all the depths and frequencies simultaneously within the homogeneous ROI, rather than averaging the local estimates across the depth axis as in (3).

Our approach allows for a fast non-iterative solution, as described in detail in the following section.

2.4. Proposed approach

The proposed linear least squares (LLS) method for the joint estimation of the attenuation and backscatter coefficients is related to the RPM, aiming to solve equations of the form (5). However, the requirement of a reference phantom in this context usually makes it difficult for use in clinical applications. In the current paper, we thus present a generalized technique that can work both in the absence and presence of a reference phantom.

While working in the absence of a reference phantom, we ignore the effects of diffraction, thereby setting $D(f, z) = 1$ in the signal model (2). This assumption is valid when one considers regions very distal to the probe, in which case ultrasound waves essentially become locally plane waves and diffraction effects can thus be neglected. These effects are also negligible when the parameter estimation is considered in the regions around the focal point of linear or phased array transducers of finite dimensions, which are commonly used in clinical applications.

In the current settings, applying a log transform to (2) results in

$$\log |S(f, z)| = \log |G\tilde{P}(f)| - 2\alpha f z + \mu \log f, \quad (9)$$

whose direct correspondence with (5) can also be observed. In equation (9), while $\tilde{P}(f)$ can be obtained by a pulse-echo reflector measurement, $G (= G' B_0)$ still needs to be estimated. In [25], where the backscatter and the diffraction terms were ignored in the signal model (2), the authors explicitly estimated G' at $z = 0$ by dividing the energy in the measured spectrum, $\tilde{S}(f, z)$ with the energy in the pulse-echo reflected spectrum, i.e. $\sum_i |\tilde{S}(f_i, 0)|^2 / \sum_i |\tilde{P}(f_i)|^2$, where $i = 1 \dots N$ for N frequency points. However, this strategy would not work in our case owing to the presence of the frequency dependent backscatter term in the model. Therefore, in addition to estimating α and μ , we propose to perform implicit calibration, by including G as an unknown variable in the estimation problem. Note that as mentioned earlier, the coefficient G is a combination of the gain calibration factor G' and the constant backscatter term B_0 . As such, B_0 cannot be estimated separately anymore as G' is not known in practice. In fact, this would also be the case even if a reference phantom would be available with the factor G' not being the same for the sample and the reference medium, in which case it would not get cancelled out in the power spectrum ratio.

Let $Q(f, z) = \log |S(f, z)| - \log |\tilde{P}(f)|$ in equation (9). We then have

$$Q(f, z) = \log G - 2\alpha f z + \mu \log f. \quad (10)$$

By stacking $Q(f, z)$ into a column vector \mathbf{q} , for all discrete values of frequencies f_i and depths z_j , and making a similar rearrangement on the right hand side of equation (10), a linear system of equations is obtained, written in vector format as

$$\mathbf{q} = \mathbf{A}\Theta. \quad (11)$$

Here,

$$\mathbf{q} = [Q(f_1, z_1) \cdots Q(f_1, z_M), Q(f_2, z_1) \cdots Q(f_2, z_M),$$

$$\cdots, Q(f_N, z_1) \cdots Q(f_N, z_M)]^T, \quad (12)$$

where $[\cdot]^T$ denotes the transpose operation and for every $i \in (1, \dots, N)$ and $j \in (1, \dots, M)$, $Q(f_i, z_j) = \log |S(f_i, z_j)| - \log |\tilde{P}(f_i)|$. Further, in equation (11),

$$\mathbf{A} = [\mathbf{1}_{MN \times 1} \quad \mathbf{a} \quad (\log \mathbf{f}) \otimes \mathbf{1}_{M \times 1}], \quad (13)$$

where for any $x \in \mathbb{R}$, $\mathbf{1}_{x \times 1}$ is a ones vector of size x ,

$$\mathbf{a} = [-2f_1 z_1, \dots, -2f_1 z_M, \dots, -2f_N z_1, \dots, -2f_N z_M]^T,$$

$\mathbf{f} = [f_1, \dots, f_N]^T$, \log is an element-wise logarithm and \otimes denotes the Kronecker product. $\Theta = [\log G \quad \alpha \quad \mu]^T$ in equation (11) represents the vector of sought parameters.

Now, replacing $S(f, z)$ in $Q(f, z)$ with the measured spectrum $\tilde{S}(f, z)$ yields $\tilde{\mathbf{q}}$, and the equality in equation (11) is not exact anymore. In this case, we propose to solve the system of linear equations in (11) in a weighted least squared error sense, resulting in the following optimization problem

$$\begin{aligned} \hat{\Theta} &= \underset{\Theta}{\operatorname{argmin}} \sum_{n=1}^{MN} w_n (\tilde{\mathbf{q}} - \mathbf{A}\Theta)_n^2, \\ &= \underset{\Theta}{\operatorname{argmin}} \|\mathbf{W}^{1/2} (\tilde{\mathbf{q}} - \mathbf{A}\Theta)\|_2^2, \end{aligned} \quad (14)$$

where the notation $(\cdot)_n$ denotes the n^{th} element of its argument vector and $\|\cdot\|_2$ denotes the ℓ_2 -norm. \mathbf{W} is a diagonal matrix with diagonal elements being the weights, $\operatorname{diag}(\mathbf{W}) = (w_1, \dots, w_{MN})$. Its role is to provide different weights to the measurement points, e.g., to downweight measurements with a strong noise component. However, studying the choice of weights is out of scope of the current manuscript, wherein we consider a uniform weighting scheme and take the weight matrix to be an identity matrix, i.e. $\mathbf{W} = \mathbf{I}_{MN}$ (weighting all the frequency-depth points equally). This reduces to

$$\hat{\Theta} = \underset{\Theta}{\operatorname{argmin}} \|\tilde{\mathbf{q}} - \mathbf{A}\Theta\|_2^2. \quad (15)$$

This is a linear least squares problem, which can be solved using standard linear algebra techniques. Its optimum value can be expressed as a closed form solution [33], written as

$$\hat{\Theta} = (\mathbf{A}^T \mathbf{A})^{-1} \mathbf{A}^T \tilde{\mathbf{q}}. \quad (16)$$

It is noted that problem (15) and its solution (16) effectively combine all the measurements at all the depth and frequency points (f and z) jointly in a single estimation problem. This is a very different approach compared to estimating α for each z independently and then averaging the results as in (3). When using all the measurements in a single estimation problem, the relationships between f and z in the backscatter model (2) can be exploited by the estimator. In Section 4, we will demonstrate that this approach leads to better estimates.

When working with a reference phantom, the aforementioned methodology would still hold. In this case, the target vector corresponds to $\Theta = [\log \tilde{B}_0 \quad \tilde{\alpha} \quad \tilde{\mu}]^T$, from which the parameters of the target tissue can be retrieved by plugging in known values of the respective parameters of the reference phantom in equations (6)-(8).

2.5. Computational complexity of LLS

Computationally speaking, the $3 \times MN$ matrix $(\mathbf{A}^T \mathbf{A})^{-1} \mathbf{A}^T$ in the closed form solution in equation (16) can be pre-computed as \mathbf{A} is independent of the measured data. This means that for LLS, the tissue parameters can be computed very efficiently in a single shot, only requiring $3(MN - 1)$ additions and $3MN$ multiplications.

3. Methods & Implementation details

3.1. Data Generation

The validation of the proposed method was conducted with simulated (synthetic) data as well as data obtained from tissue-mimicking phantoms, both without and with reference phantom measurements.

3.1.1. Synthetic Data

A medium with a depth of 40 mm was considered, consisting of a one-dimensional distribution of point scatterers positioned randomly using a uniform distribution across the full depth. The scatterers were assumed to be positioned in the far-field of a flat unfocused single element transducer. A scatterer density of approximately 50 scatterers per mm was simulated, following the Rayleigh scattering condition (i.e. > 8 scatterers/resolution cell [34]). The backscattered signal from each of the scatterers was coherently summed in the time domain to obtain a single RF line, which can be written by using the model (1) and (2) as

$$r(t) = \sum_{i=1}^{N_{sc}} \mathcal{F}^{-1} \left[P(f) e^{-2\alpha f z_i} B_0 f^\mu e^{-j2\pi f \Delta t_i} \right], \quad (17)$$

where N_{sc} is the total number of point scatterers, $\mathcal{F}^{-1}\{x\}$ represents the inverse Fourier transform of x , z_i is the position of the i th scatterer, $\Delta t_i = \frac{2z_i}{c}$ is the time delay corresponding to the position of the i th scatterer, and c is the speed of sound whose value was taken as 1500 ms^{-1} . It is to be noted that an arbitrary choice of sound speed does not affect the estimation performance. The spectrum $P(f)$ in (17) is simulated as a Gaussian spectrum of a transmit pulse with 2.25 MHz centre frequency, fractional bandwidth of 70%, and a pulse length of 2.46 mm ($1.64 \mu\text{s}$). Further, the backscattered signal was simulated for three values of the attenuation coefficients, 0.5, 1.5 and 2 dB/cm/MHz, and for each of these values, $\mu = 0.5$ and 2 was considered. The aforementioned values of α and μ are within realistic ranges [13] and were chosen to mimic the cases spanning from low to high values of these coefficients. In all the cases, B_0 was set to be $10^{-4}(\text{cm}\cdot\text{sr})^{-1}$, which is practically observed, for instance, for a healthy liver [35]. Additive white Gaussian noise was added to the time-domain backscattered signal, with a signal-to-noise ratio (SNR) of 24 dB.

A total of 500 RF lines were generated with randomly varying position of the scatterers in the medium, from which, N_{RF} RF lines were chosen for obtaining $\tilde{S}(f_i, z_j)$ by averaging the magnitudes of the spectrum obtained from individual RF lines. For each value of N_{RF} , the selection of N_{RF} RF

Table 1

The phantoms used in the experiment and their acoustic properties.

α (dB/cm/MHz)	enumeration	density (kg/m ³)	speed of sound (m/s)
0.39	1, 2	1276	1587
0.61	3, 4	1086	1546
0.63	5	1000	1552
0.63	6	1198	1596
0.71	7	1305	1518
0.84	8, 9	1100	1520

lines from the total 500 lines was repeated $N_{rep} = 10$ times to measure the variance of the estimates for a given N_{RF} . Further, the choice in each repetition was unique, so that the observation sequences remain independent.

3.1.2. In-vitro (phantom) experiments

For these experiments, the data used was taken from a previously performed study in [25], specifying all the experimental set-up and data collection details. In essence, tissue mimicking phantoms with different attenuation characteristics were prepared by mixing gelatin, agarose and poly vinyl alcohol (PVA) based gels with different concentrations of graphite powder in order to modify the attenuation characteristics of the materials and to achieve sufficient scattering. The base material of phantoms enumerated as 1, 2 and 6 as per Table 1 was PVA, and that of phantoms 3, 4, 5, and 7 was gelatin, and of phantoms 8 and 9 was agarose. The true value of the attenuation coefficient, varying over a range as presented in Table 1, was obtained using the through-transmission substitution method. It compares signal amplitudes in a medium of known attenuation, with the amplitudes obtained during the propagation through the sample. Flat unfocused single element 0.5" transducers with 65% fractional bandwidth and 10 MHz center frequency (V311-SU, Panametrics NDT, Inc., Waltham, MA) were used for the through-transmission experiment. Successive sinusoidal bursts, produced by a waveform generator (AWG NI PXI 5412, National Instruments Corporation, Austin, TX) and PC-controlled by LabVIEW, were sent in the form of a discrete frequency sweep (from 0.5 till 20 MHz with 250 kHz step), such that, at each frequency, the waveform consisted of 120 cycles. This signal was amplified (150A100B Amplifier Research, Souderton, PA) and sent to the emitting transducer. 64 transmitted signals, recorded at the receiving transducer, were digitized by means of a data acquisition card (DAQ PXI NI 5122, 14 bit, 100 MHz sampling rate, National Instruments Corporation, Austin, TX), and the averaged signal was stored on the PC. All measurements were performed at room temperature (22°C). The average speed of sound through these phantoms was 1552.4 ms^{-1} with a standard deviation of 30.94 ms^{-1} as determined experimentally.

The backscattered signals were recorded in pulse-echo mode where a single transducer was operated as emitter as well as receiver. Three different types of transducers were used for the backscatter measurements. All transducers were

flat unfocused single-element, 0.500 (13 mm) transducers: a V306-SU with a 2.25 MHz center frequency and 60% bandwidth, an A306-SU with 2.25 MHz center frequency and 50% bandwidth and a V309-SU with 5 MHz center frequency and 65% bandwidth (Panametrics NDT, Inc., Waltham, MA). In order to avoid near-field diffraction effects and to satisfy the plane-wave assumption, the phantoms were placed in a water tank in the far-field of the emitting/receiving transducer. The far-field distance for the transducers was calculated as:

$$z_{\text{far-field}} = \frac{a^2}{4\lambda} \quad (18)$$

where a is the transducer diameter (in this case 13 mm) and λ is the wavelength. Thus, using a speed of sound in distilled water at room temperature (1483 m/s), the far-field distance was calculated to be 70 mm for a 2.25 MHz transducer and 140 mm for a 5 MHz transducer. For each phantom, as many as 10 RF lines (or observation sequences) were acquired, by small displacements of the transducer in a plane parallel to the surface of the phantom in steps of 2 mm.

3.1.3. In-vitro (phantom) experiments along-with reference phantom

For the experiments with a reference phantom, the properties of the considered phantoms are presented in Table 2. Here, the backscatter coefficient values are provided in terms of the power spectrum model of the backscattered signal [31]. A detailed description of the phantom composition and the experimental set-up can be found in [26], [31], [36].

In brief, for phantom A, water-based agarose-propylene glycol mixed with filtered milk was used for the sample phantom, and agarose-based gel with graphite powder for the reference phantom. Similarly, for phantoms B and C, a mixture of water-based gelatin and ultrafiltered milk was used. Phantoms B and C were multi-layered phantoms and for these phantoms, the first layer of Phantom C was used as a reference. In all these phantoms, scattering was produced using 5-43 μm diameter thick solid glass-beads. Single-element transducers were used to obtain the ground truth values for the phantoms using the narrowband substitution method (for attenuation) and broad-band pulse-echo technique (for backscatter).

In each case, 10 uncorrelated RF data frames were acquired using a 9L4 linear array transducer on a Siemens Acuson S3000 (Issaquah, WA) with 6.6 MHz center frequency for phantom A, and a 18L6 linear array transducer on a Siemens Acuson S2000 scanner with 8.9 MHz center frequency for phantom B and C.

3.2. Data Processing

To test the performance of our method on the RF data, MATLAB was used. In order to compute the magnitude spectrum, the time-domain RF signal was divided into overlapping segments, as shown in the top plot of fig. 1. The magnitude spectrum of the signal within each window was computed after multiplying it with a Hanning window, to minimize spectral leakage. Moreover, in each j th sliding window, the obtained magnitude spectra for the considered

Table 2

Acoustic properties of the sample and reference phantoms used in the reference phantom measurement experiments. Only the RF data from the first layer was used for multi-layered phantoms B and C.

Label	Phantom	α (dB/cm/MHz)	$B'_0 (= B_0^2)$ (cm-sr-MHz μ') $^{-1}$	μ' ($= 2\mu$)
A	Sample	0.654	1.02e-06	4.16
	Reference	0.670	8.79e-06	3.14
B	Sample	0.554	4.82e-07	3.80
	Reference	0.510	1.60e-06	3.52
C	Sample	0.510	1.60e-06	3.52
	Reference	0.510	1.60e-06	3.52

N_{RF} RF lines² were then averaged to be finally used as the measured spectra $\tilde{S}(f, z_j)$ for the window centered around the depth point z_j . Further, this spectrum was evaluated only over a usable frequency band as shown using the blue line in the bottom plot of fig. 1. Using this data, the performance of the proposed approach was assessed for various choices of the window length, window overlap, and usable bandwidth using analysis and validation studies, as described below.

3.3. Benchmark method for comparison

As a benchmark, we consider the dynamic programming (DP) based methodology that has been proposed in [28]. In this work, the authors exploited the depth-continuity of the tissue parameters in a regularized cost function. ℓ_2 and later, ℓ_1 regularization [29] was considered to enforce this continuity of the parameters of interest across the depth axis, where the latter was shown to exhibit superior performance. The resultant cost function was solved iteratively using DP and the method was shown to provide better estimates than those obtained by the least squares method in [26]. More importantly, the adopted DP method benefitted from optimizing the parameters at different depths together, rather than treating each depth independently as done in [25]-[26].

To compare the DP method with our approach on the considered data sets, the implementation details for the DP method are as follows. First, while in the original paper, the authors considered a RPM based model (such as in equation (5)), here when working in the absence of a reference phantom, the model was adapted as done in our approach in equation (10). Second, the regularized cost function consisted of a data fidelity term and an ℓ_1 regularization term for each of the three parameters of interest, associated with their regularization weights. We set the regularization weights to 10^8 , which were found to give the best estimates on the considered data sets³. Finally, DP requires specifying the search ranges for each of the parameters to be estimated (thereby in-

²For phantom data using reference phantom measurements, around 40 RF lines were considered in each RF data frame.

³For the considered homogeneous medium settings, large value of this regularization parameter ensures that the parameters of interest (α and μ) do not vary much across the depth axis. This implies that a strong smoothness regularization is beneficial to obtain good estimates.

Table 3

Tabulation of factors that influence the attenuation and backscatter estimates, which are used in the ANOVA for comparison of means.

Variable	Value	Description
N_{RF}	10, 50	Number of RF lines
ME	LLS	Proposed LLS method
	DP	Dynamic Programming method
α_{true}	0.5, 2	Low and high values of the attenuation coefficient in dB/cm/MHz
μ_{true}	0.5, 2	Low and high values of the frequency dependent backscatter term

roducing a trade-off between prior knowledge and estimation accuracy). We used the following ranges- (i) for α estimation with true α value α_{true} : $\alpha_{true} - 0.3 \leq \alpha \leq \alpha_{true} + 0.3$, (ii) for μ estimation with true μ value μ_{true} : $\mu_{true} - 0.3 \leq \mu \leq \mu_{true} + 0.3$ (for phantom data without considering a reference phantom, μ_{true} was unknown and μ was varied between its physical range of 0 and 2) and (iii) for G estimation: it was swept between one lower and one higher order of magnitude than its expected magnitude, as obtained by explicit calibration⁴ [25].

3.4. Statistical Analysis

A statistical analysis using analysis of variance (ANOVA) test was performed, which is commonly used to analyze if there exists any statistically significant differences between the means of more than two independent groups. In the current context, we used four-way ANOVA, where the continuous dependent variables were the relative error of the attenuation and backscatter estimates, influenced predominantly by four categorical independent variables: the number of RF lines used (N_{RF})⁵, the method of estimation (ME), the true value of α (α_{true}) and μ (μ_{true}). These variables and their respective values are presented in Table 3.

In order to obtain the p -values for the four variables, the function `anovan` in MATLAB was used. For the posthoc analysis, if appropriate, to primarily identify the influence of ME , α_{true} and μ_{true} on the relative error, the function `multcompare` was used.

3.5. Sensitivity to parameter settings

A parameter sensitivity study was performed to analyze the effect of three parameters, namely the sliding window length, the window overlap and the usable bandwidth on the accuracy of the estimates of the sought coefficients.

⁴For phantom data using reference phantom measurements, $\alpha_{true} = (\alpha_s - \alpha_r)_{true}$, $\mu_{true} = (\mu_s - \mu_r)_{true}$ and G corresponds to $((B_0)_s / (B_0)_r)_{true}$.

⁵In general, N_{RF} can take any number of possible values. Here, for the sake of statistical analysis, we make it a categorical variable by considering N_{RF} to be either 10 or 50.

3.5.1. Influence of window length

As the window length increases, the number of samples used to compute the spectrum $\tilde{S}(f, z)$ increases, which increases the spectral resolution. However, according to the Heisenberg-Gabor uncertainty principle in time-frequency analysis, this reduces the spatial resolution as it becomes more ambiguous at which depth the spectrum is actually analyzed, thereby creating inaccuracies in the depth-related attenuation model. Hence, there exists a trade-off in the choice of the window length. The optimal window length can be found empirically by plotting the relative estimation errors, both for α : $|\alpha_{true} - \hat{\alpha}| / \alpha_{true}$ and μ : $|\mu_{true} - \hat{\mu}| / \mu_{true}$, as a function of the window length, using the simulated data for different values of α_{true} and μ_{true} .

3.5.2. Influence of window overlap

For a fixed window length, the larger the overlap between successive windows, the more z -observations can be used in the least squares estimation. This may increase accuracy, yet with a larger computational cost.

3.5.3. Influence of usable bandwidth

The term usable bandwidth refers to the frequency range of the spectrum that is above the noise floor and over which the model is fitted. If the usable bandwidth is too small, the number of samples used for estimating α and μ is too small resulting in a poor estimation performance. If the usable bandwidth is too large, the accuracy of the estimates might decrease since large values of the bandwidth might capture the noise-dominated parts of the spectrum.

3.6. Effect of Depth Information

To emphasize the importance of considering the full depth information in the model, we performed tests for the coefficients estimation by applying LLS with and without full depth inclusion. The former corresponds to the proposed approach in this paper, whereas the latter corresponds to obtaining an estimate for each sliding window separately using LLS, followed by averaging all such estimates over the whole depth as in (3).

3.7. Computation time analysis

The computation time of the proposed LLS method is a crucial factor for its real-time implementation in clinical settings. An empirical study was performed to analyze the influence of the various parameters on the time taken by LLS to provide the coefficients' estimates. For each parameter setting, the computation time was measured for 10 repeated attenuation and backscatter computations in MATLAB, after which the average time and standard deviations were computed over these 10 trials.

4. Results

4.1. Proposed technique vs DP

In fig. 2, the relative errors of the α and μ estimates using LLS and DP, based on the simulated data, are plotted as a function of the number of RF lines (N_{RF}), for two cases with

LLS for attenuation and backscatter estimation

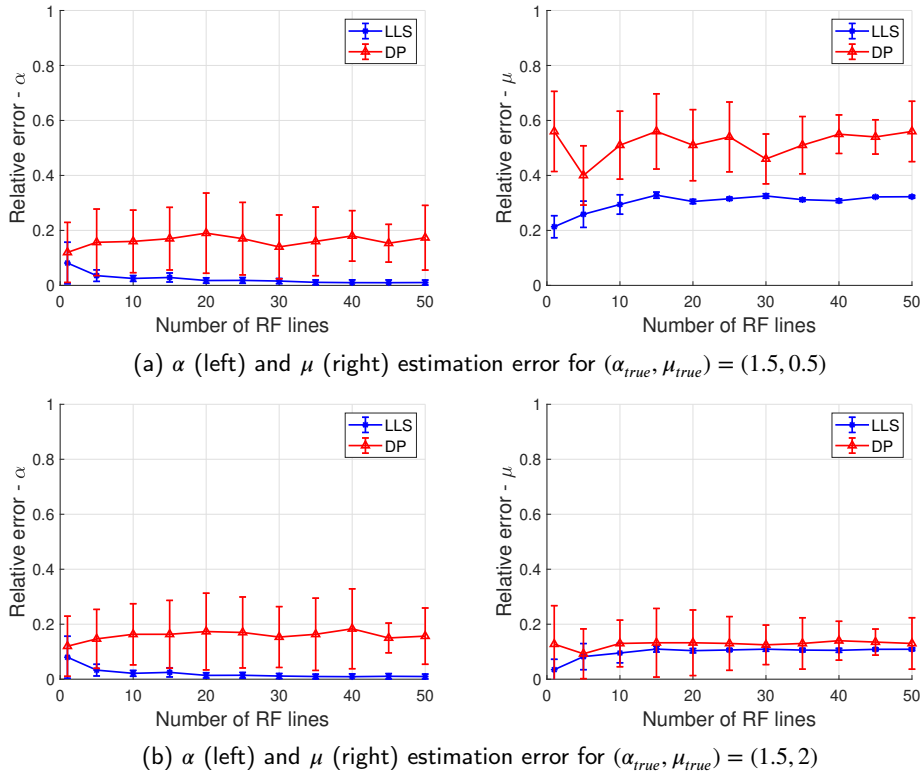


Figure 2: The relative error of the α and μ estimates using LLS and DP is plotted, for cases with $(\alpha_{true}, \mu_{true}) = (1.5, 0.5)$ in the first row and $(\alpha_{true}, \mu_{true}) = (1.5, 2)$ in the second row, as a function of the number of RF lines N_{RF} , used to make an observation sequence. For each N_{RF} value, the mean relative error is plotted, in which the error bars show the standard deviation of the errors when the experiment is repeated $N_{rep} = 10$ times. In all the cases, the window length chosen (4.92 mm) is twice the pulse-length of the transmitted pulse, the window overlap is 90% and the usable bandwidth (1.57 MHz) is equal to the bandwidth of the transmitted pulse.

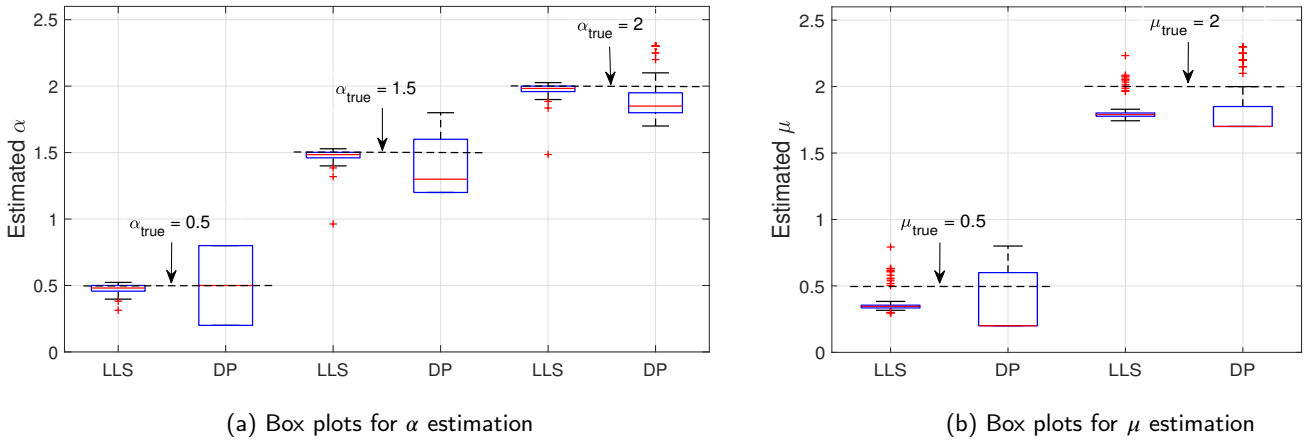


Figure 3: Box plots representing (a) α and (b) μ estimates over all values of N_{RF} , obtained by LLS and DP. (a) shows the box plots for estimated α for the cases with $\alpha_{true} = 0.5, 1.5$ and 2 , with $\mu_{true} = 2$. Similarly, (b) depicts the box plots for estimated μ for the cases with $\mu_{true} = 0.5$ and 2 , with $\alpha_{true} = 1.5$. Outliers (defined by the MATLAB 'boxplot' function) are indicated as red '+'s.

different α_{true} and μ_{true} values (for space considerations, all other cases are provided in the supplementary material). The estimates were obtained by using a sliding window technique with the optimal settings of the window length, window overlap and usable bandwidth, as observed from the parameter

sensitivity analysis (section 4.3). From the figure, it can be seen that LLS provides estimates with lower relative estimation error than DP. Another point of appreciation is that for LLS, the variance is comparatively low and the trend is more or less flat for $N_{RF} > 10$. As mentioned earlier, in the

Table 4

Tabulation of p -values and mean errors as obtained by posthoc analysis on relative error of α estimates with respect to different categorical variables.

Variable	Value	Mean relative error	p -value
ME	LLS	0.032 ± 0.063	0.0003
	DP	0.494 ± 0.063	
α_{true}	0.5	0.428 ± 0.063	0.0035
	2	0.098 ± 0.063	
μ_{true}	0.5	0.262 ± 0.063	0.9856
	2	0.264 ± 0.063	

Table 5

Tabulation of p -values and mean errors as obtained by posthoc analysis on relative error of μ estimates with respect to different categorical variables.

Variable	Value	Mean relative error	p -value
ME	LLS	0.176 ± 0.042	0.0024
	DP	0.407 ± 0.042	
α_{true}	0.5	0.225 ± 0.042	0.0464
	2	0.358 ± 0.042	
μ_{true}	0.5	0.463 ± 0.042	0.0001
	2	0.120 ± 0.042	

absence of a reference phantom, the constant term B_0 can not be found as the estimated factor G will also be influenced by the (unknown) gain calibration factor G' . As such, all the results in the absence of a reference phantom are shown only for α and μ estimates.

For further comparison between the two approaches, the estimated values are shown as a box plot in fig. 3, considering all values of N_{RF} and 10 repeated runs for each N_{RF} , for different values of α_{true} and μ_{true} . The figure depicts a lower spread in the estimated values in each case over all considered runs for LLS than that obtained for DP. Additionally, for LLS, the overall trend is that the median of the box plot is closer to the true value of the coefficient under investigation, which suggests that LLS leads to more accurate estimates.

4.2. Statistical Analysis

The influence of the variables listed in Table 3 on the relative error of the coefficients estimates was statistically analyzed using the ANOVA test. On the one hand, the obtained p -values for N_{RF} were greater than the level of significance of 5% for both α and μ relative errors, indicating no significant difference in the mean errors with respect to N_{RF} . On the other hand, the p -values for the rest of the categorical variables were observed to be below the level of significance and these cases were thus further analyzed using a posthoc analysis. Its results are reported in Table 4 and 5 for α and μ , respectively. Several observations can be made from the presented values. First, the mean error is smaller for LLS than DP for both α and μ estimates. Second, the accuracy of the α estimate depends on the α_{true} value. Lastly, the μ_{true} value affects the accuracy of the μ estimation.

4.3. Sensitivity to parameter settings

The results are shown for the case $(\alpha_{true}, \mu_{true}) = (1.5, 2)$ in fig. 4 (all the other cases are provided in the supplementary material).

First, it can be observed from fig. 4(a) that DP is more sensitive to the choice of the window length than the LLS method. From these plots (as well as the other cases in the supplementary material), it is found that a window size of twice the pulse length (4.92 mm in this case) is a good choice in general, leading to the lowest errors. Second, in fig. 4(b), the relative error of the estimates does not vary much by varying window overlap from 0% to 90%. Finally, in fig. 4(c), the usable bandwidth was varied from a very small value (~ 0.2 MHz) to around 2.25 MHz, which would be the bandwidth of the transmitted pulse if the transducer's relative bandwidth was taken to be 100%. In these plots, the relative error reduces around 1.57 MHz, which also corresponds to the bandwidth of the considered transmitted pulse (in units of dB, it is 6 dB below the peak of the spectrum).

4.4. Effect of Depth Information

Fig. 5 shows the relative errors of α and μ estimates obtained using LLS with the cases when the full depth information was accounted for in the model ('LLS' labelled case in the plots) and when the estimates were instead obtained by averaging the local estimates across the depth axis ('avgd. LLS' labelled case in the plots) as in (3). The shown cases are with $(\alpha_{true}, \mu_{true}) = (1.5, 0.5)$ in the top row and $(\alpha_{true}, \mu_{true}) = (1.5, 2)$ in the bottom row (since all the cases show a similar trend, only two such cases are shown here). The values of the window length, window overlap and usable bandwidth were optimized to get the least relative error for the parameters estimated in the avgd. LLS case. Even by doing so, these plots demonstrate the superior performance of the proposed model, which combines frequency and depth information, in reducing the relative estimation error. Moreover, this difference in relative error is more pronounced for α estimation, which has a depth dependency in the modelled spectrum, than for μ estimation.

4.5. Computation time analysis

One of the main advantages of our method is its low computational cost. In terms of MATLAB computation time, while LLS executed each case in the order of seconds, DP took time in the order of several hours (note that this depends largely on the resolution of the search grid for each sought parameter. A finer search grid could provide more accurate estimates, but at the cost of even higher computation time).

Further, three key parameters were found to be largely influencing the LLS computation time: the number of RF lines, the window overlap and the window length. The influence of N_{RF} and the window overlap on the time is depicted in fig. 6 for LLS implementation in MATLAB R2020a for the case with $(\alpha_{true}, \mu_{true}) = (1.5, 2)$ (other cases also show a similar trend), setting window length to twice the transmitted pulse-length. It can be seen that the time taken by LLS for coefficients estimation (with matrix $(\mathbf{A}^T \mathbf{A})^{-1} \mathbf{A}^T$ pre-computed,

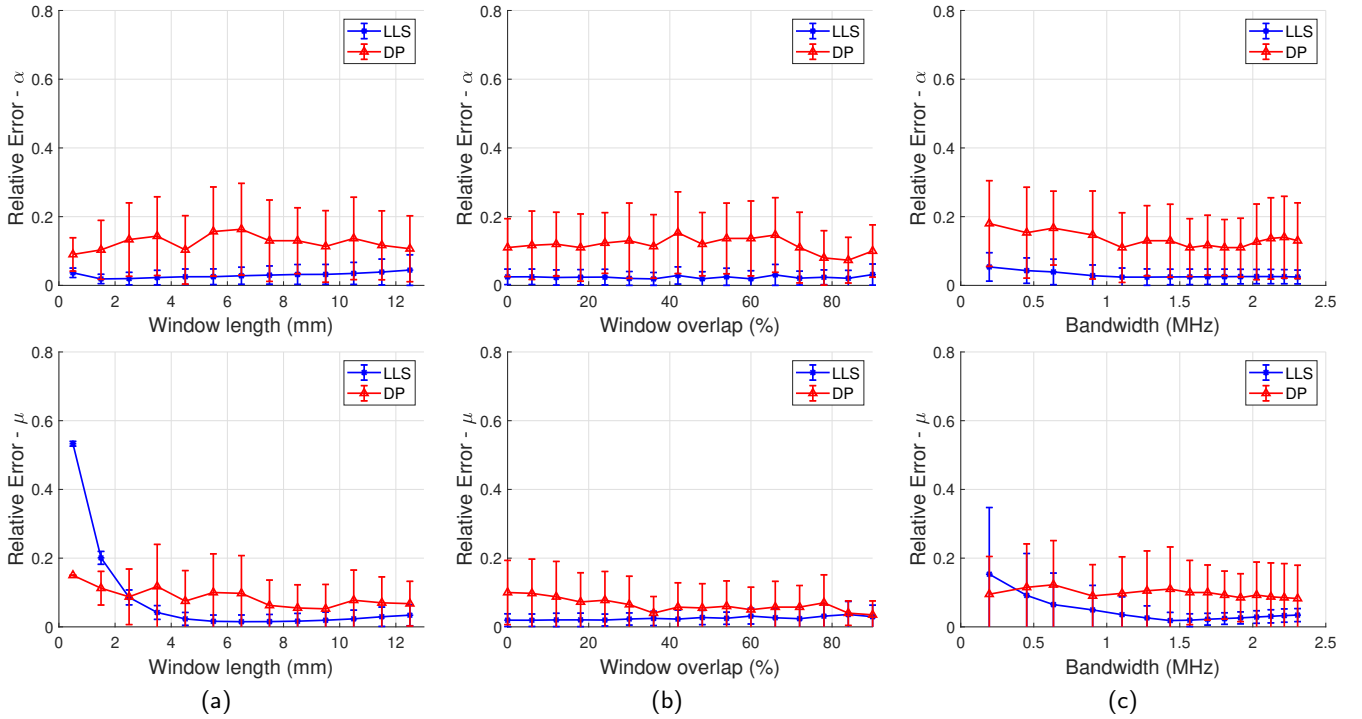


Figure 4: The relative errors of the α and μ estimates, where $N_{RF} = 50$ and $(\alpha_{true}, \mu_{true}) = (1.5, 2)$, using LLS and DP are plotted against: (a) window length, (b) window overlap and (c) usable bandwidth. In each case, the mean relative error is plotted, in which the error bars show the standard deviation of the errors when the experiment is repeated $N_{rep} = 10$ times. For (a), the window overlap is 90% and the usable bandwidth (1.57 MHz) is equal to the bandwidth of the transmitted pulse. For (b), the window length chosen (4.92 mm) is twice the pulse-length of the transmitted pulse and the usable bandwidth (1.57 MHz) is equal to the bandwidth of the transmitted pulse. For (c), the window length chosen (4.92 mm) is twice the pulse-length of the transmitted pulse and the window overlap is 90%.

see section 2.5) is reduced by ~ 75 -80% by changing N_{RF} from 50 to 10 and window overlap from 90% to 50%, without worsening the estimation accuracy (fig. 2 and fig. 4(b), respectively).

Concerning the window length, any reduction in the LLS computation time by increasing the window length came at the cost of increased coefficient estimation error. This is in accordance with earlier observations that the LLS performance is more sensitive to the choice of the window length than of other parameters. Moreover, for the already low computation time point, i.e., $N_{RF} = 10$ and 50% window overlap, increasing the window length was not observed to give an appreciable time reduction. Therefore, it was kept fixed to twice the transmitted pulse-length to maintain the estimates high accuracy.

4.6. Attenuation Estimates with in-vitro (sample phantom) data

In fig. 7, the relative error for the attenuation estimates from phantom data is shown by means of a bar diagram. It can be observed that the overall accuracy of our method is better than the DP method. More precisely, the relative error of the estimates, averaged over all the phantoms, was 16% for LLS, compared to 51% for DP.

The overall trend for the LLS estimates can be seen nearly in line with the statistical analysis on the simulated data,

showing a decrease in the relative error as the α_{true} value increases from phantom 1 to 8, where phantom 9 could be viewed as an outlier. It is to be noted that the ground-truth values for μ in the phantoms were not known. Consequently, the relative errors on the μ estimation could not be computed and only the results for α estimation are shown.

4.7. Attenuation & Backscatter Estimates with in-vitro (sample & reference phantoms) data

The bar diagram in fig. 8 presents the relative error for the attenuation estimates from the phantom data using reference phantom measurements. These plots depict the higher accuracy achieved by our method than the DP method for the attenuation coefficient estimation. In particular, the relative error of the attenuation estimates, averaged over all the phantoms, was 5% for LLS, compared to 10% for DP. The estimates of the backscatter coefficient computed over the transducer's bandwidth are shown in fig. 9. It can be observed that while LLS outperforms DP for phantom A, both methods perform reasonably well in the estimation of the backscatter coefficient spectrum for the other two phantoms.

Finally, it can be noticed that the α_{true} values for the three phantoms are comparable and predicting any difference in their relative errors based on the statistical analysis might not be suitable here.

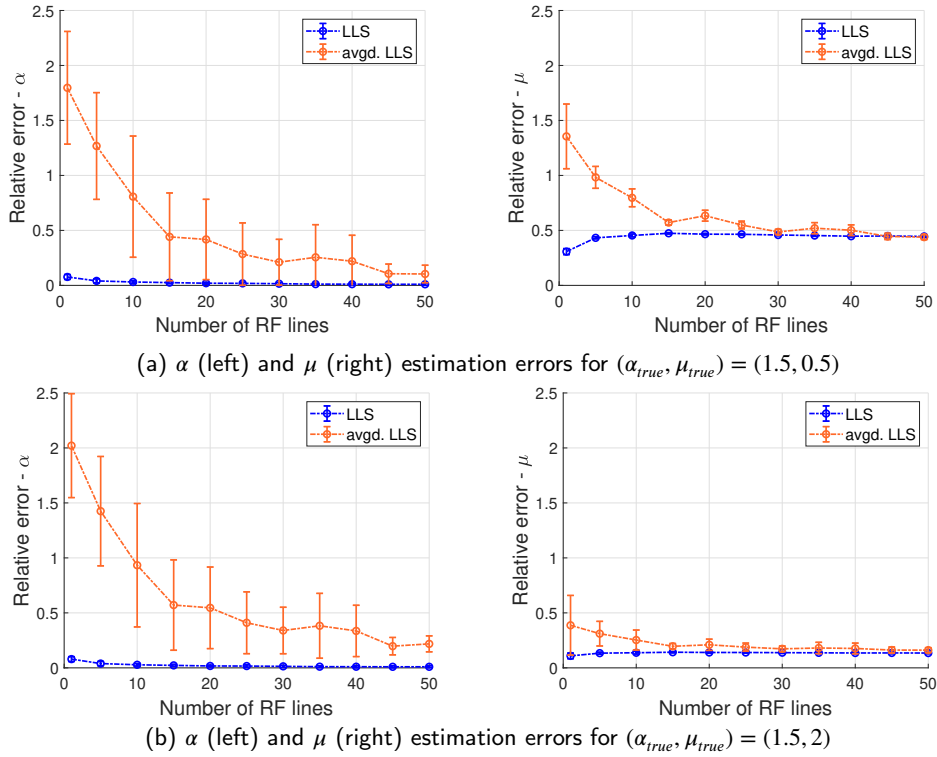


Figure 5: The relative error of the α and μ estimates using LLS is plotted, for cases with $(\alpha_{true}, \mu_{true}) = (1.5, 0.5)$ in the first row and $(\alpha_{true}, \mu_{true}) = (1.5, 2)$ in the second row, against the number of RF lines, N_{RF} . For each N_{RF} value, the mean relative error is plotted, in which the error bars show the standard deviation of the errors when the experiment is repeated $N_{rep} = 10$ times. The plots avgd. LLS show the relative error of the estimates obtained by averaging the estimates from each depth (window) as in (3). The plots LLS show the relative error of the estimates obtained by including the depth information in the estimation framework, providing a global estimate, as proposed in this manuscript. In all the cases, the window length chosen is 6 mm, the window overlap is 75% and the usable bandwidth is 2.4 MHz.

5. Discussion

We have presented a new approach for fast and accurate estimation of ultrasound attenuation and backscatter coefficients. In general, one of the key differences between our approach and the existing least squares based methods in the literature relates to the solver we have proposed here. In our case, the heaviest calculations to be performed by the solver are independent of the data, such that they can be pre-computed offline, which makes the method very useful for real-time applications. This single-shot non-iterative estimator is in contrast with other techniques that employ iterative solvers [26], or suffer from high computation cost [28]. Additionally, our method combines both the frequency and depth dimension in a single estimation problem, providing a global estimator for all the depths combined in contrast to the averaging of independent local estimators in other approaches.

For validation, we compared our method with the DP method in [28], which benefits from using a regularization term to enforce piece-wise continuity of the parameters of interest across the depth axis. As indicated by the performed studies, our method provided more accurate estimates than DP. While DP intrinsically smoothens the local estimates at different depths (thereby coupling them to each other), our approach is designed to obtain a single parameter esti-

mation for all depths exploiting the dependency of z in the model, which conceptually is a very different approach. It might be one of the reasons why more accurate estimation results are obtained by our approach on the considered data sets. Furthermore, an important distinction is a much higher computational cost of DP, making it unsuited for real-time processing. Another point worth highlighting here is that DP requires a search range to be specified for each of the sought parameter. This range is typically considered to be within some vicinity of the expected true value. However, this dependency on search range has several drawbacks. If the parameter's true value is not known precisely, a very wide search range would have to be explored. Additionally, for higher accuracy, a fine gridding of the search space would need to be considered. Either of these scenarios would make this approach computationally very expensive. Contrary to this, our method does not rely on any such prior information in the form of a pre-defined search range and provides the estimates much faster with a computational complexity of only $3MN$ multiplications/additions for a grid with N frequency points and M depth-points.

For statistical analysis, the ANOVA test was performed on the relative errors of the estimated coefficients, which validated the previous observation of the proposed LLS method

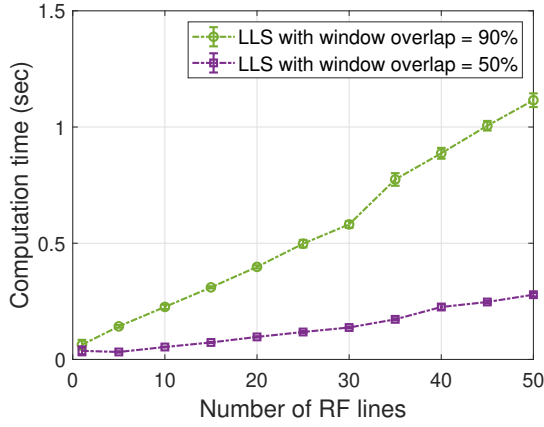


Figure 6: Plots of time taken by LLS for coefficients estimation as a function of number of RF lines, N_{RF} , for the synthetic data case with $(\alpha_{true}, \mu_{true}) = (1.5, 2)$, considering window overlap of 90% (green curve) and 50% (purple curve), both with a window length of twice the transmitted pulse-length. For each N_{RF} value, the mean time taken (in seconds) is plotted, in which the error bars show the standard deviation of the time taken when the experiment is repeated $N_{rep} = 10$ times. The shown times correspond to an LLS implementation in MATLAB R2020a.

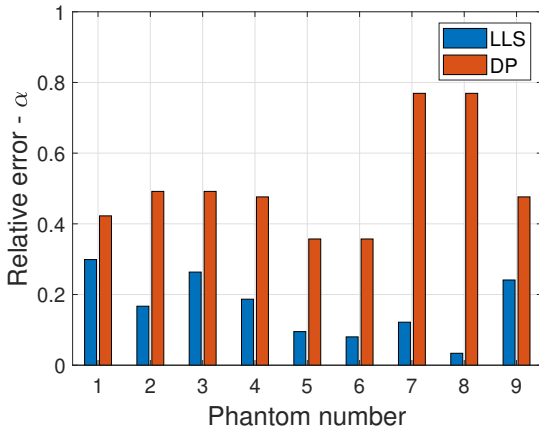


Figure 7: Bar diagram of the relative errors of attenuation coefficient estimates for each of the nine tissue-mimicking phantoms, using LLS and DP.

outperforming the DP method. Further analysis showed that the estimation accuracy of the methods depends on the true values of the coefficients. Higher values of the α_{true} provided (relatively) more accurate α estimates when compared to the lower values (see Table 4). One possible reason is that at higher values of attenuation coefficient, the effect of the attenuation on the spectrum is more pronounced. Similarly, higher μ_{true} led to better estimation of μ , which could again be due to its more notable influence on the spectrum than when its true value is lower. Further, no appreciable effect of μ_{true} value was seen on the α estimation and vice versa.

The sensitivity of α and μ estimates was also studied with respect to the parameters used in the formation of the spectra: the window length, the window overlap and the usable bandwidth. The results suggested that a window length

of twice the transmitted pulse-length is a good choice in general. LLS was also seen to be less sensitive to the window length than DP, indicating the reliability of the LLS method over a wide range of parameter settings. Keeping the window length fixed, the analysis on the window overlap indicated that the estimation accuracy is fairly robust to the choice of this parameter. Further analysis on the usable bandwidth showed that an optimum value could be set close to the bandwidth of the transmitted pulse. In fact, in all the cases and for all parameter settings, the estimation error of LLS remained always lower than or on par with the estimation errors of the DP method.

Another analysis pertained to the inclusion of depth information in the model. Since the proposed LLS framework directly captures the attenuation effects as a function of depth and frequency jointly, the estimates were more accurate than the estimates obtained by locally averaging the coefficient estimates at each depth, as shown in fig. 5.

The analysis performed on the LLS computation time indicated that a time reduction can be achieved while keeping the same estimation accuracy by considering smaller values of N_{RF} and the window overlap. This is expected as these parameters influence the number of spectra (Fast Fourier Transforms) to be computed, which is the computational bottleneck of LLS. While keeping the window length fixed to twice the transmitted pulse-length, 10 RF lines with 50% window overlap were seen to be achieving computation time of the order of 10^{-2} seconds. Varying the window length for these settings did not exhibit any further reduction in time. It is noted that the computation time heavily depends on the hardware and software that is used, such that its values (as depicted in Fig. 6) should not be interpreted in the absolute sense. They merely give an impression of the time it takes to compute this on a personal computer in MATLAB. Faster times are achievable with dedicated hardware and with hardware-software co-development strategies. This highlights the possibility of integrating LLS into ultrasound systems for real-time coefficient estimation.

The coefficients estimation results on the simulated data were verified with the phantom data both with and without reference phantom measurements. As evident from figs. 7-8, LLS performed better than DP, providing attenuation estimates with lower relative error. The two methods are also shown to provide backscatter coefficient estimates in agreement with the respective true values in fig. 9.

Looking ahead to apply our method in clinical settings, a few things are highlighted here. First, since the estimation errors obtained by LLS exhibited low error variance for each N_{RF} and an almost flat trend for $N_{RF} > 10$ (see fig. 2), it indicates the potential of LLS to provide accurate estimates even from data acquired using only few RF lines. This could be particularly beneficial in clinical settings as for few RF lines, only a small lateral size of the ROI would need to be probed. Moreover, such a lateral size would also result into achieving higher spatial resolution when building QUS parametric images.

Second, the proposed strategy could be generalized to

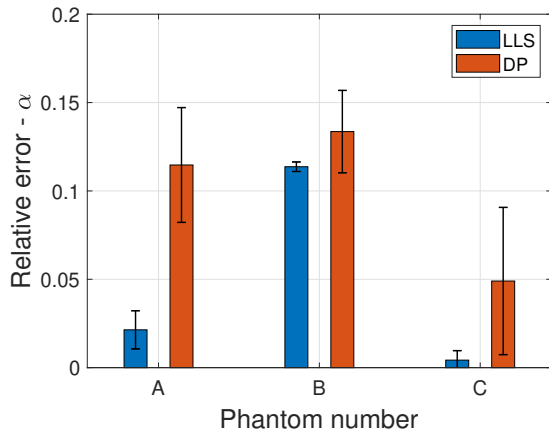


Figure 8: Bar diagram of the mean relative errors of attenuation coefficient estimates for each of the three tissue-mimicking phantoms with the respective reference phantom measurements, using LLS and DP. The error bars show the standard deviation of the relative errors obtained for 10 RF data frames.

incorporate weights in our model (see equation (14)). The purpose of the resultant weighted linear least squares problem would be to account for the noise usually present in realistic scenarios, which could help in better estimations of the parameters of interest. Typically, the weights are chosen by taking the reciprocal of the noise variance at each measurement point. Alternatively, in the current context, the weights could be specified for each depth point, covering all the frequency points or vice versa, as per the error variance at these points. The choice of the weights should, however, be studied.

Finally, an ultimate testing of the proposed methodology needs to be performed in-vivo. In this context, when a homogeneous ROI is of clinical interest [39], the proposed LLS method could be directly applied for the coefficient estimation. However, when the heterogeneity of the underlying tissue needs to be captured by building its attenuation and backscatter coefficient maps, a generalization of our method towards a heterogeneous, i.e. multi-layered, tissue model would be required. While this is beyond the scope of the current paper, we note that a first step towards such an extension was presented in [30]. This will be further developed in future work.

6. Conclusion

A fast linear least squares (LLS) estimation of the attenuation and backscatter coefficient has been proposed in this paper. The proposed approach exploits frequency and depth information jointly to provide accurate estimates at a low computational effort, making it applicable in real-time imaging settings. Comparison with a state-of-the-art DP method on simulated and phantom data has shown that our approach outperforms DP both in accuracy and computational efficiency. The estimates obtained using the LLS method are shown to exhibit less variability with respect to the window length and the overlap between the consecutive windows. It also has

a lower relative estimation error for the considered usable bandwidth range.

Supplementary material

See online supplementary material for figures showing the relative error of coefficient estimation plots for all the considered cases of α_{true} and μ_{true} values, supplementing figs. 2 and 4.

Acknowledgment

The authors would like to thank Dr. Natalia Ilyina for providing the experimental data for the phantoms without reference phantom measurements. The authors would further like to thank Prof. Timothy J Hall, Hayley Whitson (University of Wisconsin) and Dr. Ivan Rosado (Instituto de Física-UNAM) for providing the reference phantom measurements based experimental data. The authors acknowledge the financial support of the European Union's Horizon 2020 research and innovation programme under grant agreement No.766456 (project AMPHORA).

References

- [1] F.L. Lizzi, M. Greenebaum, E.J. Feleppa, M. Elbaum, and D.J. Coleman, "Theoretical framework for spectrum analysis in ultrasonic tissue characterization", *J. Acoust. Soc. Am.*, vol. 73(4), pp.1366-1373, 1983.
- [2] B.S. Garra, M.F. Insana, T.H. Shawker, and M.A. Russell, "Quantitative estimation of liver attenuation and echogenicity: normal state versus diffuse liver disease", *Radiology*, 162(1), pp.61-67, 1987.
- [3] M.F. Insana, T.J. Hall, J.G. Wood, Z.Y. Yan, "Renal ultrasound using parametric imaging techniques to detect changes in microstructure and function", in *Invest Radiol.*, 28:720-25, 1993.
- [4] E.J. Feleppa, S. Urban, A. Kalisz, F.L. Lizzi, W.R. Fair, C.R. Porter, "Advanced ultrasonic imaging of the prostate for guiding biopsies and for planning and monitoring therapy", in *Proc. IEEE Ultrason. Symp.*, 2:1399-403, 2000.
- [5] Y. Fujii, N. Taniguchi, K. Itoh, K. Shigeta, Y. Wang, J. W. Tsao, K. Kumasaki and T. Itoh "A new method for attenuation coefficient measurement in the liver: Comparison with the spectral shift central frequency method", *J. Ultrasound Med.* vol. 21 no. 7 pp. 783-788 2002.
- [6] P. A. Narayana and J. Ophir, "On the Frequency Dependence of Attenuation in Normal and Fatty Liver", in *IEEE Trans. Sonics Ultrason.*, vol. 30, no. 6, pp. 379-382, Nov. 1983.
- [7] S. K. Jeon, J. M. Lee, I. Joo, J. H. Yoon, D. H. Lee, J. Y. Lee, and J. K. Han, "Prospective Evaluation of Hepatic Steatosis Using Ultrasound Attenuation Imaging in Patients with Chronic Liver Disease with Magnetic Resonance Imaging Proton Density Fat Fraction as the Reference Standard", *Ultrasound Med. Biol.*, vol. 45, no. 6, pp. 1407-1416, June 2019
- [8] K. A. Wear, "Characterization of trabecular bone using the backscattered spectral centroid shift," in *IEEE Trans. Ultrason., Ferro-electr., Freq. Control*, vol. 50, no. 4, pp. 402-407, April 2003.
- [9] M. Sasso, G. Halat, Y. Yamato, S. Naili, and M. Matsukawa, "Dependence of ultrasonic attenuation on bone mass and microstructure in bovine cortical bone", in *J. Biomech.* vol. 41, pp. 347-355, 2008.
- [10] F. Deeba, M. Ma, M. Pesteie, J. Terry, D. Pugash, J. A. Hutcheon, C. Mayer, S. Salcudean and R. Rohling, "Attenuation Coefficient Estimation of Normal Placentas", in *Ultrasound Med. Biol.*, vol. 45, no. 5, pp. 1081-1093, 2018
- [11] X. Li and D.C. Liu, "Estimation of local attenuation and its application to rationalized gain control", in *1st Int. Conf. Bioinformatics and Biomedical Engineering, IEEE*, pp. 1249-1252, July, 2007.

LLS for attenuation and backscatter estimation

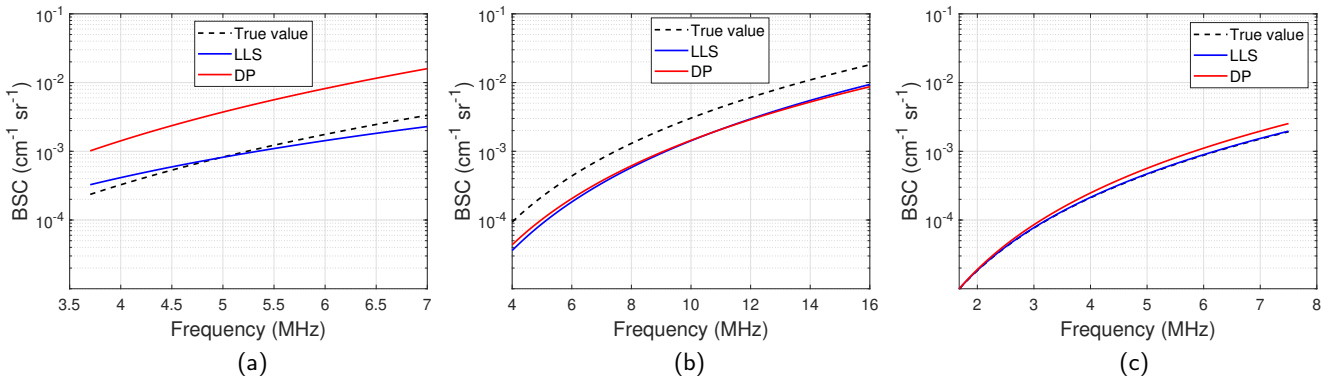


Figure 9: Backscatter coefficient (BSC) estimation of sample (a) phantom A, (b) phantom B and (c) phantom C, using the data with reference phantom measurements. In each plot, true values are shown along with the estimated values using LLS and DP.

- [12] T. Liu, F. L. Lizzi, R. H. Silverman, and G. J. Kutcher, "Ultrasonic tissue characterization using 2-D spectrum analysis and its application in ocular tumor diagnosis", in *Med. Phys.* vol. 31, no. 15, pp. 1032-1039, 2004.
- [13] K. Nam, J.A. Zagzebski, and T.J. Hall, 2013, "Quantitative assessment of in vivo breast masses using ultrasound attenuation and backscatter", in *Ultrasonic imaging*, 35(2), pp.146-161, 2013.
- [14] S.D. Pye, S.R. Wild and W.N. McDicken, "Adaptive time gain compensation for ultrasonic imaging", in *Ultr. Med. Bio.*, 18(2), pp.205-212, 1992.
- [15] R. Kuc, M. Schwartz, and L. Von Micsky, "Parametric estimation of the acoustic attenuation coefficient slope for soft tissue", in *Proc. IEEE Ultrason. Symp. (IUS)*, Sep./Oct. 1976, pp. 44-47
- [16] P. A. Narayana and J. Ophir, "On the validity of the linear approximation in the parametric measurement of attenuation in tissues", *Ultrasound Med. Biol.*, vol. 9, no. 4, pp. 357-361, 1983
- [17] H. Kim and T. Varghese, "Attenuation estimation using spectral cross-correlation", *IEEE Trans. Ultrason., Ferroelectr., Freq. Control*, vol. 54, no. 3, pp. 510-519, Mar. 2007
- [18] Z. Klimonda, M. Postema, A. Nowicki, and J. Litniewski, "Tissue Attenuation Estimation by Mean Frequency Downshift and Bandwidth Limitation", *IEEE Trans. Ultrason., Ferroelectr., Freq. Control*, vol. 63, no. 8, pp. 1107-1114, May 2016.
- [19] R. Kuc and M. Schwartz, "Estimating the acoustic attenuation coefficient slope for liver from reflected ultrasound signals", *IEEE Trans. Sonics Ultrason.*, vol. 26, no. 5, pp. 353-361, Sep. 1979.
- [20] M. Insana, J. Zagzebski, and E. Madsen, "Improvements in the spectral difference method for measuring ultrasonic attenuation", *Ultrason. Imag.*, vol. 5, no. 4, 331-345, 1983.
- [21] R. Kuc, "Estimating acoustic attenuation from reflected ultrasound signals: Comparison of spectral-shift and spectral-difference approaches", *IEEE Trans. Acoust., Speech, Signal Process.*, vol. 32, no. 1, pp. 1-6, Feb. 1984.
- [22] L. X. Yao, J. A. Zagzebski, and E. L. Madsen, "Backscatter coefficient measurements using a reference phantom to extract depth-dependent instrumentation factors", *Ultrason. Imag.*, vol. 12, no. 1, pp. 58-70, 1990
- [23] H. Kim, and T. Varghese, "Hybrid spectral domain method for attenuation slope estimation", *Ultrasound Med. Biol.*, vol. 34, pp. 1808-1819, 2008.
- [24] K. Samimi, and T. Varghese, "Optimum diffraction-corrected frequency-shift estimator of the ultrasonic attenuation coefficient", *IEEE Trans. Ultrason. Ferroelectr. Freq. Control*, vol. 63(5), pp.691-702, 2016.
- [25] N. Ilyina, J. Hermans, E. Verboven, K. Van Den Abeele, E. D'Agostino and J. D'hooge, "Attenuation estimation by repeatedly solving the forward scattering problem", *Ultrasonics*, vol. 84, pp. 201-209, 2018.
- [26] K. Nam, J. A. Zagzebski, and T.J. Hall, "Simultaneous backscatter and attenuation estimation using a least squares method with constraints", *Ultrasound Med. Biol.*, vol. 37, pp. 2096-2104, 2011.
- [27] A.L. Coila, and R. Lavarello, "Regularized spectral log difference technique for ultrasonic attenuation imaging", *IEEE Trans. Ultrason. Ferroelectr. Freq. Control*, vol. 65(3), pp.378-389, 2017.
- [28] Z. Vajjhi, I.M. Rosado-Mendez, T.J. Hall, and H. Rivaz, "Low variance estimation of backscatter quantitative ultrasound parameters using dynamic programming", *IEEE Trans. Ultrason. Ferroelectr. Freq. Control*, vol. 65(11), pp.2042-2053, 2018.
- [29] Z. Vajjhi, I. Rosado-Mendez, T.J. Hall, and H. Rivaz, "L1 And L2 Norm Depth-Regularized Estimation Of The Acoustic Attenuation And Backscatter Coefficients Using Dynamic Programming", *In 2019 IEEE 16th Int. Symp. Biomed. Imaging (ISBI 2019)*, pp. 1749-1752, 2019.
- [30] A. Muraleedharan, A. Bertrand, and J. D'hooge, "A Linear Least Squares Estimation of Spatially Variant Attenuation from Ultrasound Backscatter Signals", in *Proc. Mtgs. Acoust.*, Acoustical Society of America, 38, 020016 (2019).
- [31] N. Jafarpisheh, T.J. Hall, H. Rivaz and I.M. Rosado-Mendez, "Analytic Global Regularized Backscatter Quantitative Ultrasound", *IEEE Trans. Ultrason. Ferroelectr. Freq. Control*, doi: 10.1109/TUFFC.2020.3042942, 2020.
- [32] J. Nocedal and S. J. Wright (1999), *Numerical Optimization*, Springer Series in Operations Research, Springer, Berlin
- [33] G. Strang, *Linear Algebra and its Applications*, Thomson, Brooks/Cole (2006)
- [34] G. Georgiou and F. S. Cohen, "Statistical characterization of diffuse scattering in ultrasound images", in *IEEE Trans. Ultrason., Ferroelectr., Freq. Control*, vol. 45, no. 1, pp. 57-64, Jan. 1998.
- [35] Z.F. Lu, J.A. Zagzebski, and F.T. Lee, "Ultrasound backscatter and attenuation in human liver with diffuse disease", in *Ultrasound Med. Biol.*, vol. 25, no. 7, pp.1047-1054, 1999.
- [36] K. Nam, I.M. Rosado-Mendez, L.A. Wirtzfeld, G. Ghoshal, A.D. Pawlicki, E.L. Madsen, R.J. Lavarello, M.L. Oelze, J.A. Zagzebski, W.D. O'Brien Jr, and T.J. Hall, "Comparison of ultrasound attenuation and backscatter estimates in layered tissue-mimicking phantoms among three clinical scanners", *Ultrason. Imag.*, 34(4), pp.209-221, 2012.
- [37] S. W. Flax, N. J. Pelc, G. H. Glover, F. D. Gutmann, and M. McLachlan, "Spectral characterization and attenuation measurements in ultrasound", *Ultrason. Imag.*, vol. 5, no. 2, pp. 95-116, 1983.
- [38] D. Nicholas, "Evaluation of backscattering coefficients for excised human tissues: Results interpretation and associated measurements", *Ultrasound Med. Biol.*, vol. 8, pp. 17-28, 1982
- [39] F. Deeba, M. Ma, M. Pesteie, J. Terry, D. Pugash, J.A. Hutcheon, C. Mayer, S. Salcudean and R. Rohling, "Attenuation coefficient estimation of normal placentas", in *Ultrasound Med. Biol.*, 45(5), pp.1081-1093, 2019